

Article

Luminescent Hydrogel Based on Silver Nanocluster/Malic Acid and Its Composite Film for Highly Sensitive Detection of Fe³⁺

 Xiangkai Liu ^{1,2}, Chunhui Li ^{1,2} , Zhi Wang ¹, Na Zhang ^{1,*}, Ning Feng ¹, Wenjuan Wang ¹ and Xia Xin ^{1,*} 

¹ Key Laboratory of Colloid and Interface Chemistry (Ministry of Education), School of Chemistry and Chemical Engineering, Shandong University, Jinan 250100, China; lxk575730669@163.com (X.L.); li_chunhui0411@163.com (C.L.); zwang@mail.sdu.edu.cn (Z.W.); 202020302@mail.sdu.edu.cn (N.F.); wenjuanwang@mail.sdu.edu.cn (W.W.)

² China Research Institute of Daily Chemistry Co., Ltd., Taiyuan 030001, China

* Correspondence: nzhang@sdu.edu.cn (N.Z.); xinxs@sdu.edu.cn (X.X.)

Abstract: Metal nanoclusters (NCs) with excellent photoluminescence properties are an emerging functional material that have rich physical and chemical properties and broad application prospects. However, it is a challenging problem to construct such materials into complex ordered aggregates and cause aggregation-induced emission (AIE). In this article, we use the supramolecular self-assembly strategy to regulate a water-soluble, atomically precise Ag NCs (NH₄)₉[Ag₉(C₇H₄SO₂)₉] (Ag₉-NCs, [Ag₉(mba)₉], H₂mba = 2-mercaptobenzoic acid) and L-malic acid (L-MA) to form a phosphorescent hydrogel with stable and bright luminescence, which is ascribed to AIE phenomenon. In this process, the AIE of Ag₉-NCs could be attributed to the non-covalent interactions between L-MA and Ag₉-NCs, which restrict the intramolecular vibration and rotation of ligands on the periphery of Ag₉-NCs, thus inhibiting the ligand-related, non-radiative excited state relaxation and promoting radiation energy transfer. In addition, the fluorescent Ag₉-NCs/L-MA xerogel was introduced into polymethylmethacrylate (PMMA) to form an excellently fluorescent film for sensing of Fe³⁺. Ag₉-NCs/L-MA/PMMA film exhibits an excellent ability to recognize Fe³⁺ ion with high selectivity and a low detection limit of 0.3 μM. This research enriches self-assembly system for enhancing the AIE of metal NCs, and the prepared hybrid films will become good candidates for optical materials.

Keywords: silver nanoclusters; malic acid; self-assembly; AIE; sensor



Citation: Liu, X.; Li, C.; Wang, Z.; Zhang, N.; Feng, N.; Wang, W.; Xin, X. Luminescent Hydrogel Based on Silver Nanocluster/Malic Acid and Its Composite Film for Highly Sensitive Detection of Fe³⁺. *Gels* **2021**, *7*, 192. <https://doi.org/10.3390/gels7040192>

Academic Editor: Hiroyuki Takeno

Received: 28 September 2021

Accepted: 26 October 2021

Published: 31 October 2021

Publisher's Note: MDPI stays neutral with regard to jurisdictional claims in published maps and institutional affiliations.



Copyright: © 2021 by the authors. Licensee MDPI, Basel, Switzerland. This article is an open access article distributed under the terms and conditions of the Creative Commons Attribution (CC BY) license (<https://creativecommons.org/licenses/by/4.0/>).

1. Introduction

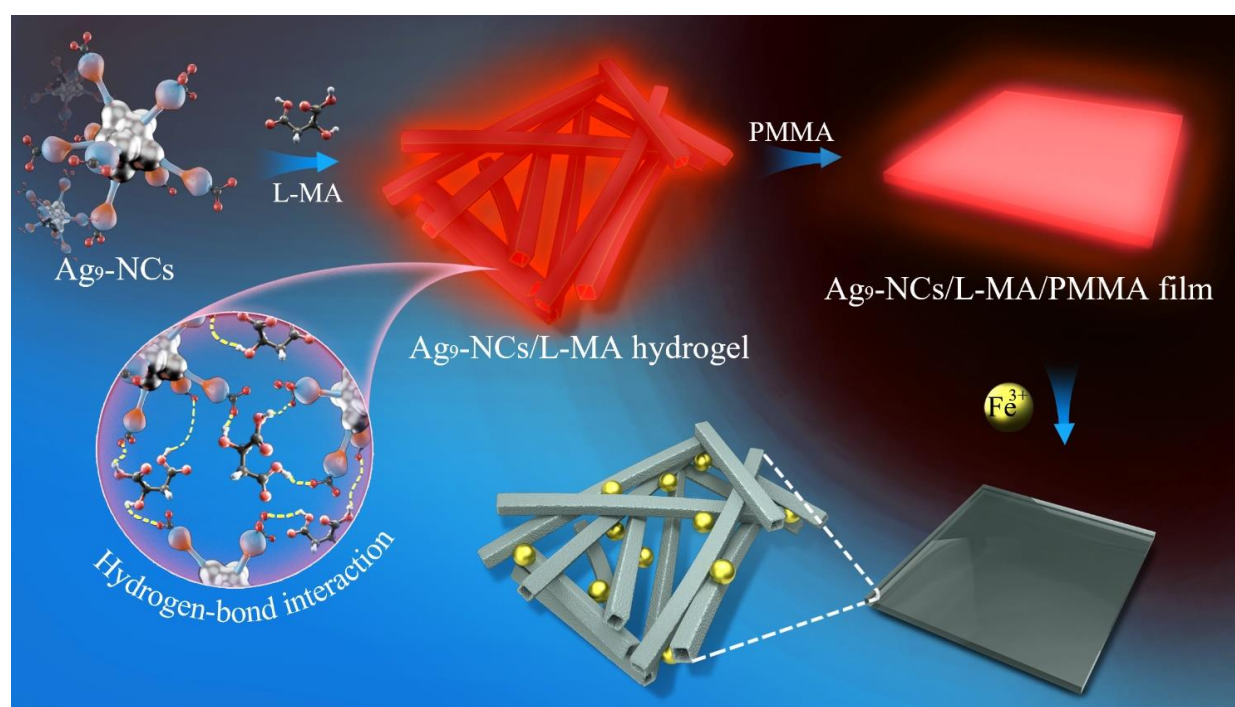
Metal nanoclusters (NCs), such as gold, silver, and copper NCs, represent a class of multifunctional materials with attractive optoelectronic and photoluminescence properties [1–5]. It consists of a metal core, composed of several to hundreds of metal atoms and a peripheral organic ligand, forming a unique core-shell structure [6–10]. Due to their large Stokes shift, low toxicity, good biocompatibility, and other excellent characteristics, metal NCs can be used as environmentally friendly and biocompatible color conversion materials, fluorescent probes, and excellent biological probe for protein expression [11–19].

Recently, the aggregation-induced emission (AIE) strategy has been used to enhance the photoluminescence of metal NCs, thereby enhancing its application in fluorescent sensing, light-emitting diodes, and other optoelectronic devices [20–22]. At present, the commonly used methods for AIE are solvent and cation-induced aggregation. However, these two methods cannot obtain ordered aggregates, resulting in instability and poor uniformity of nanocluster aggregation [23–26]. Therefore, an effective strategy for manipulating the spatial arrangement of nanostructured units to form a specific structure: self-assembly, was introduced to solve this problem. By regulating the non-covalent forces between multiple molecules (van der Waals forces, hydrogen bonds, electrostatic interactions, and π - π stacking), metal NCs, and other molecules form ordered aggregates with specific functions, which further improves the photoluminescence performance of the metal NCs [27–29].

For example, Shen et al. used the supramolecular self-assembly strategy to obtain stable colloidal aggregates (nanospheres and nanovesicles) of $\text{Ag}_6\text{-NCs/PEI}$, through multiple electrostatic interactions between $\text{Ag}_6\text{-NCs}$ and polyethyleneimine (PEI) [30]. During the formation of the order structure, the $\text{Ag}_6\text{-NCs}$ luminescence in the dilute aqueous solution was turned on. Zhang et al. demonstrated the enhancement of the luminescence of Cu NCs by forming compact and ordered self-assembly architectures by changing the annealing temperature in the formation of Cu NCs [31]. Therefore, it can be seen that the self-assembly of metal NCs is very attractive and worth studying.

Fluorescent film sensors are widely considered, due to their advantages, such as convenient portability, real-time detection, and no pollution to the system, for testing [32–37]. Compared with the solution and powder detection forms, the adjustable shape, size, and flexibility of the fluorescent film makes it have wider application prospects. For example, Li et al. optimized the concentration of octadecylamine with amino groups in n-hexane to make the Tris-base modified silver NCs self-assemble into a single-layer silver nanocomposite film at the n-hexane-water interface and use it as a surface enhancement Raman scattering (SERS) active substrate for ultra-sensitive detection of Hg^{2+} ions [38]. The SERS sensing monolayer film also has good reproducibility and recovery rate. Katowah et al. used an in-situ method to prepare a ternary nanocomposite film containing copper oxide/polymethylmethacrylate (PMMA)/various carbon-based nanofillers, as a selective Hg^{2+} ion sensor and the mixed nanofiller significantly improved performance of PMMA film [39].

Herein, a water-soluble, atomically precise Ag NCs ($(\text{NH}_4)_9[\text{Ag}_9(\text{C}_7\text{H}_4\text{SO}_2)_9]$ ($\text{Ag}_9\text{-NCs}$, $[\text{Ag}_9(\text{mba})_9]$, $\text{H}_2\text{mba} = 2\text{-mercaptobenzoic acid}$, and the molecular structure of $\text{Ag}_9\text{-NCs}$ is shown in Figure S1) were selected to self-assembled with L-malic acid (L-MA) to construct phosphorescent hydrogels (Scheme 1). The $\text{Ag}_9\text{-NCs/L-MA}$ hydrogel has a hollow-tube structure which is regulated by non-covalent interactions, based on hydrogen bonds, which further promotes the AIE phenomenon. In order to further develop its application prospects as fluorescent sensors, $\text{Ag}_9\text{-NCs/L-MA}$ xerogels are doped into PMMA films to construct fluorescent film sensors for detecting Fe^{3+} ions. The value of the corresponding quenching coefficient, K_{SV} , is $5.2 \times 10^4 \text{ M}^{-1}$ in the low concentration range, and the detection limit of Fe^{3+} is down to $0.3 \mu\text{M}$.



Scheme 1. Schematic illustration of the hollow-tube structure of $\text{Ag}_9\text{-NCs/L-MA}$ hydrogel and its composite film for highly sensitive detection of Fe^{3+} .

2. Results and Discussion

2.1. Self-Assembly of Ag₉-NCs/L-MA Hydrogels

The Ag₉-NCs in an aqueous solution is in a nonfluorescent state. In order to regulate the aggregation behavior and AIE of Ag₉-NCs, though the non-covalent interaction force dominated by hydrogen bonds, L-MA with hydroxyl and carboxyl functional groups is selected as a hydrogen bond donors, and Ag₉-NCs, with carboxylate on the periphery, act as hydrogen bond acceptors. Firstly, phase behavior study on Ag₉-NCs/L-MA mixed system was performed. Based on our previous study [40,41], $c_{\text{Ag}_9\text{-NCs}}$ was fixed at 8 mM, while $c_{\text{L-MA}}$ was changed. It can be seen that different phase behaviors of the samples were obtained (Figure 1a). Compared with the solution without fluorescence (0~0.1 M L-MA) and the sample in the two-phase with weaker fluorescence intensity (0.1~0.25 M L-MA), the hydrogel with higher luminous intensity (0.25~0.5 M L-MA) was selected as the main research object. Once the hydrogels formed, the UV absorption exhibits a broad peak from 200 to 550 nm (Figure 1d) and the electrons of the benzene ring system and C=O undergo $\pi\text{-}\pi^*$ and $n\text{-}\pi^*$ transitions, resulting in ultraviolet absorption bands. Moreover, orange-red fluorescence at 628 nm was excited by blue light at 470 nm (Figure 1d) and it can be observed that as $c_{\text{L-MA}}$ increases, the fluorescence intensity of the hydrogel first increases and then decreases (Figure 1e,f). This is attributed to the fact that when $c_{\text{Ag}_9\text{-NCs}} = 8$ mM and $c_{\text{L-MA}} = 0.3$ M, Ag₉-NCs and L-MA self-assemble to form highly ordered aggregates, and L-MA sufficiently limits the ligands of Ag₉-NCs, while when $c_{\text{L-MA}}$ is too high or too low, the uniformity of the formed aggregates is poor, and the self-assembly strategy cannot be effectively implemented, which leads to the weakening of fluorescence intensity. Thus, 8 mM Ag₉-NCs/0.3 M L-MA hydrogel, which has the highest fluorescence intensity was selected as the typical sample.

Then, the dynamic change of fluorescence intensity with the hydrogel formation was also studied. Once Ag₉-NCs and L-MA mixed, under the drive of non-covalent interaction forces, the fluorescent intensity of 8 mM Ag₉-NCs/0.3 M L-MA hydrogel increased immediately within 30 min, achieving AIE effect. After about 1 h, the self-assembly process is almost complete, the fluorescence intensity stabilized and no longer changed (Figure 1g,h). Moreover, the peak position of the fluorescence spectrum has a slight blue shift with time. It is speculated that Ag₉-NCs, L-MA and water molecules gradually formed the hydrogel through the hydrogen bonds, the vibration of the peripheral ligand of Ag₉-NCs is restricted, and ligand-to-metal charge transfer occurred, resulting in a blue shift of the peak position. Thus, the AIE phenomenon of Ag₉-NCs/L-MA hydrogel can be attributed to the limited intramolecular vibration and rotation of the ligand of Ag₉-NCs, which inhibits the ligand-related non-radiative excited state relaxation and promotes radiation energy transfer. Furthermore, the average of lifetime of Ag₉-NCs solution is 3.277 ns, while the average of the lifetime of 8 mM Ag₉-NCs/0.3 M L-MA hydrogel increased to 7.4383 μs (Figure 1i, Table S1), which is approximately 2270 times that of Ag₉-NCs solution. Therefore, the large Stokes shift (158 nm) and microsecond lifetime (7.4383 μs) indicate that it is essentially phosphors. Besides, the quantum yield of 8 mM Ag₉-NCs/0.3 M L-MA hydrogel, measured using the integrating sphere, is 11.20%, which is higher than that of aggregates formed by the assembly of Ag₉-NCs with other substances [42]. Longer fluorescence lifetime and higher quantum yield of Ag₉-NCs/L-MA hydrogels make it excellent candidates for luminescent sensing materials.

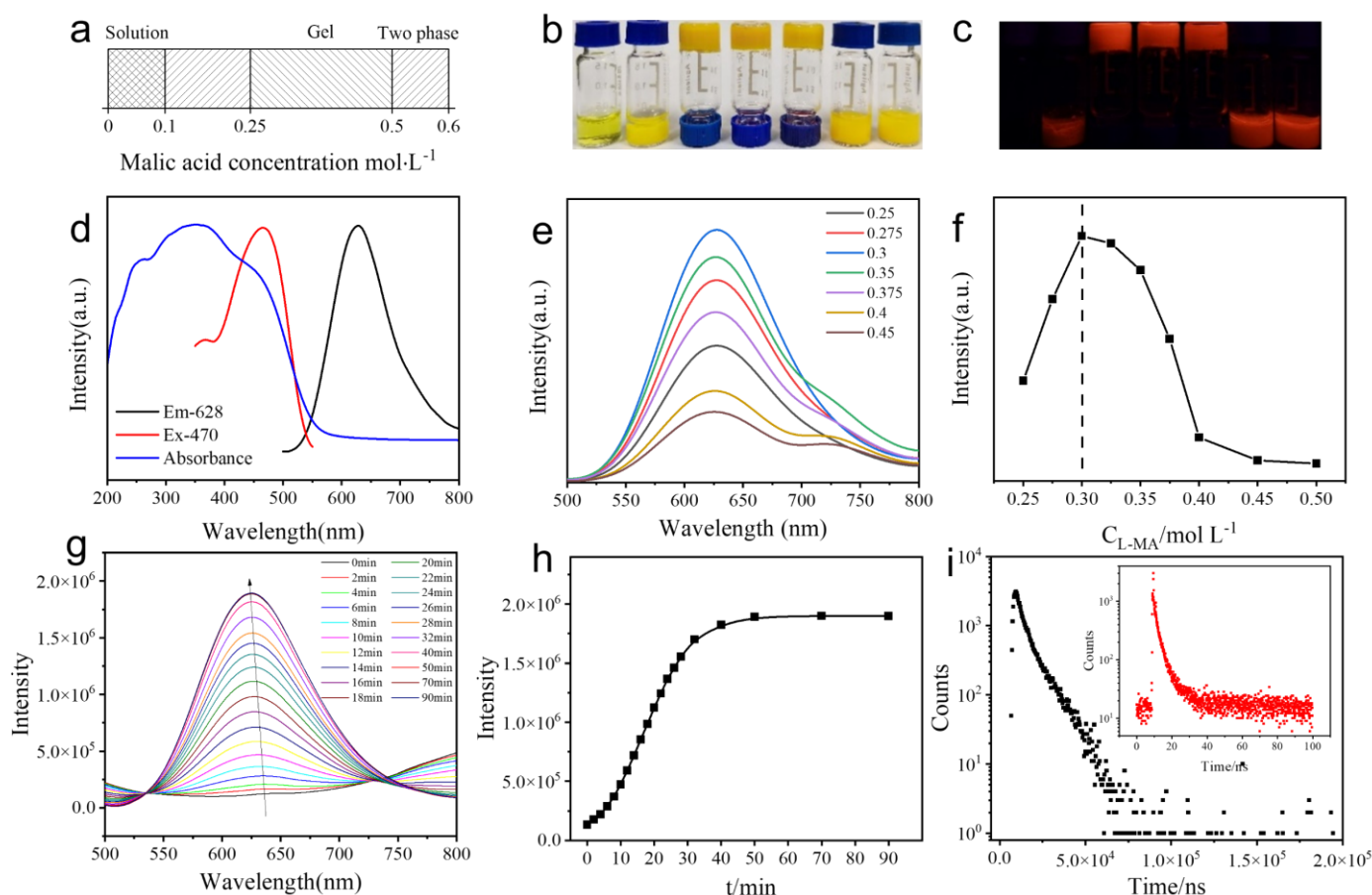


Figure 1. (a) Phase transition with different concentration of L-MA. (b) Photographs of the hydrogels with different L-MA concentrations. (c) Fluorescence photographs of the hydrogels with different L-MA concentrations. (d) Photoexcitation (red line, emission = 628 nm), photoemission (black line, excitation = 470 nm) spectra of Ag₉-NCs hydrogels, and UV-vis absorption (blue line). (e) Photoluminescence (PL) spectra of hydrogels with different concentration of L-MA for excitation at 470 nm. (f) Comparison of the luminescence intensity of hydrogels with different concentration of L-MA at 628 nm. (g) PL spectra of Ag₉-NCs hydrogels with different incubation times for excitation at 470 nm. (h) Comparison of the luminescence intensity of hydrogels with different incubation times. (i) PL decay profiles of Ag₉-NCs hydrogel. Inset: the PL decay profiles of the powder of lyophilized Ag₉-NCs solution.

Scanning electron microscopy (SEM) and transmission electron microscope (TEM) microscopic observations show that the hydrogel is composed of tangled hollow tubes with a very high aspect ratio (20:1), and most of the tubes are between 1–2 μm in length and about 50–100 nm in diameter (Figure 2a–f and Figure S2). The confocal laser scan microscopy (CLSM) image shows that the tubes structure is accompanied by strong fluorescent properties. Further observation by TEM shows that these hollow tubes are composed of a large number of smaller diameter fibers (10–20 nm) (Figure S3). Moreover, it can be seen in SEM that a small amount of hollow tubes are entangled to form a spiral (Figure 2d). It is speculated that the appearance of AIE can be attributed to the appearance of ordered hollow tube structure. The detailed formation mechanism of the hollow-tube structure of Ag₉-NCs/L-MA hydrogel can be shown in Scheme 1.

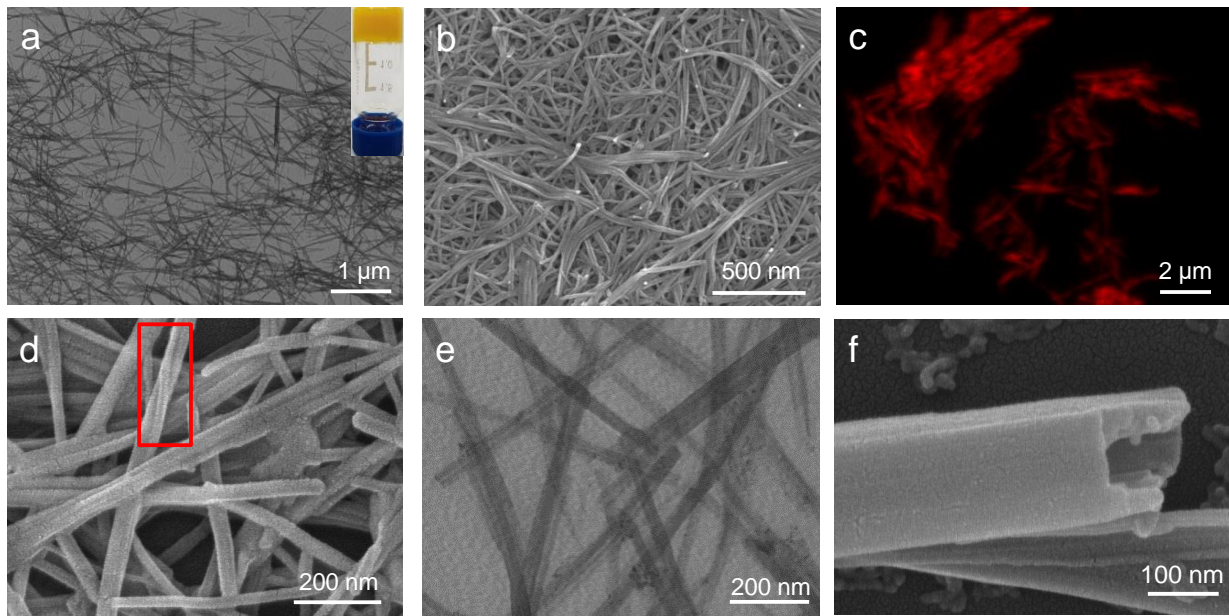


Figure 2. (a,e) TEM, (c) CLSM, and (b,d,f) SEM images of the hollow tubes of 8 mM Ag₉-NCs/0.3 M L-MA hydrogel with different magnifications (the inset of a is a photograph of the hydrogels).

2.2. Structural Analysis of the Hydrogel

In order to further analyze the mechanism of supramolecular self-assembly, a series of characterizations were carried out. Thermogravimetric analyses (TGA) can be used to measure the thermal stability of the studied substances (Figure 3a). The decomposition temperature of L-MA is about 145 °C and the decomposition temperature of the H₂mba ligand of Ag₉-NCs is about 200 °C. After assembly, the decomposition temperature of the H₂mba ligand of Ag₉-NCs for Ag₉-NCs/L-MA xerogel is about 260 °C, indicating that the stability of Ag₉-NCs is further improved by supramolecular self-assembly.

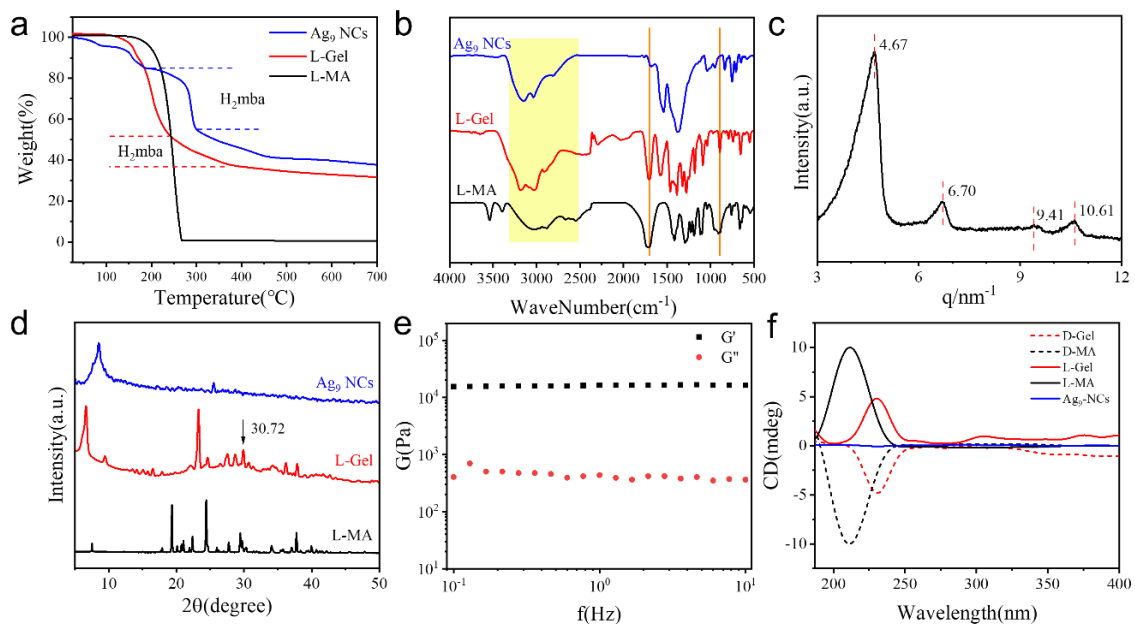


Figure 3. (a) TGA and (b) FT-IR spectra of lyophilized Ag₉-NCs solution, L-MA and Ag₉-NCs/L-MA xerogel. (c) SAXS results of Ag₉-NCs/L-MA xerogel. (d) XRD results of lyophilized Ag₉-NCs solution, L-MA and Ag₉-NCs/L-MA xerogel. (e) Variation of elastic modulus (G') and viscous modulus (G'') as a function of frequency ($\tau = 10$ Pa). (f) CD spectra of Ag₉-NCs solution, L-MA, Ag₉-NCs/L-MA hydrogels, D-MA and Ag₉-NCs/D-MA hydrogels.

Fourier transform infrared (FT-IR) is an effective tool for analyzing the supramolecular forces (Figure 3b). The broad peak of Ag₉-NCs/L-MA xerogel at 2500 cm⁻¹ to 3200 cm⁻¹ represents the stretching vibration of the hydroxyl group, which is stronger and wider than that of Ag₉-NCs, indicating the formation of hydrogen bonds in the system. The peak at 1700 cm⁻¹ representing the stretching vibration of the C=O in the carboxyl group becomes weaker than that of L-MA after the gel is formed, and slightly shifts to a lower wave number, which represents the formation of hydrogen bonds and confirms that L-MA participates in the construction of the hydrogel. The peak at 3540 cm⁻¹ represents that the hydroxyl groups in L-MA undergo intermolecular association through hydrogen bonds to form L-MA dimers, which disappear after gelation, indicating that L-MA forms hydrogen bonds with the peripheral ligands of Ag₉-NCs. The peaks at 1537 cm⁻¹ and 1377 cm⁻¹ belong to the antisymmetric and symmetric stretching vibration of C=O in carboxylate from ligand of Ag₉-NCs. For Ag₉-NCs/L-MA xerogel, the peak of C=O in carboxylate moves, which further confirms the formation of hydrogen bonds between ligand of Ag₉-NCs and L-MA. Moreover, it can be seen that the absorption peak at 900 cm⁻¹, representing O-H in the carboxyl group of L-MA is strong and after the hydrogel is formed, this peak becomes weaker and narrower, confirming that most of the carboxyl groups of L-MA are involved in the formation of hydrogen bonds, limiting the bending vibration of the O-H bonds in the carboxyl groups.

Small-angle X-ray spectroscopy (SAXS) and X-ray diffraction (XRD) can effectively characterize the deposition pattern and spatial structure of the xerogels. SAXS shows that Ag₉-NCs/L-MA xerogel exhibits four scattering peaks, and the scattering factor *q* ratio is 1 : $\sqrt{2}$: 2 : $\sqrt{5}$, which is a tetragonal stack (Figure 3c). The smallest repeating unit of the aggregate *d* = 1.36 nm (*d* = 2 π /*q*), which is equivalent to the size of Ag₉-NCs. From the XRD results, it can be observed that L-MA is a triclinic crystal system, while the peak of Ag₉-NCs/L-MA xerogel at 2 θ = 20–40° represents various possible regular arrangements of atomic layers in assembled nanostructures, which is very different from L-MA and Ag₉-NCs (Figure 3d), indicating Ag₉-NCs and L-MA formed a multi-complex during the self-assembly. According to the Bragg equation, the interplanar distances of the atomic layer are in the range of 2.37–3.81 Å. Diffraction peaks at 2 θ = 30.72 correspond to Ag-Ag, indicating that the d10-d10 argentophilic interaction may exist in the Ag₉-NCs/L-MA xerogel [40,41,43].

The rheological characteristics are of great significance for supramolecular hydrogels, and the mechanical strength of the Ag₉-NCs/L-MA hydrogels can be evaluated by the rheological measurement. In the stress scanning (Figure 3e), the storage modulus (*G'* = 16,900 Pa) is much larger than the loss modulus (*G''* = 614.6 Pa), indicating that the hydrogels exhibit a solid-like nature. The Ag₉-NCs/L-MA hydrogels exhibit good viscoelasticity, a wider linear viscoelastic region, and a higher yield stress (892.8 Pa), indicating that the hydrogels constructed by the Ag₉-NCs are more rigid and exhibit strong damage resistance. In the frequency sweep test (Figure S4), *G'* is larger than *G''* and the moduli of the hydrogels are almost independent of the applied frequency. The above results indicate that the Ag₉-NCs/L-MA hydrogels have high mechanical strength.

The circular dichroism (CD) spectrum has further confirmed that the Ag₉-NCs/L-MA hydrogel possesses supramolecular chirality. L-MA has a positive Cotton effect at 212 nm and no obvious CD signal was detected in the Ag₉-NCs aqueous solution. But the Ag₉-NCs/L-MA hydrogel has a positive Cotton effect at 230 nm, and the original CD signal of L-MA disappears. Moreover, we also used D-MA to construct Ag₉-NCs/D-MA hydrogel and it is interesting to find that the CD spectrum of the Ag₉-NCs/D-MA hydrogel is exactly opposite of the Ag₉-NCs/L-MA hydrogel. It can be concluded that through supramolecular self-assembly, the molecular chirality of L-MA (or D-MA), was successfully transferred to the supramolecular level, which induced the Ag₉-NCs/L-MA hydrogel (Ag₉-NCs/D-MA hydrogel) has supramolecular chirality (Figure 3f).

2.3. Ag₉-NCs/L-MA Xerogel/PMMA Film for Sensing

The composite material obtained by doping the xerogel into the polymer matrix has the advantages of easy processing and good flexibility and can enhance the practical application of the gel [32,33]. PMMA has good UV resistance, chemical durability, and good mechanical properties. Therefore, based on the excellent sensing performance of metal NCs and the advantages of simple preparation of organic films as a matrix material, Ag₉-NCs/L-MA xerogel are introduced into the organic glass matrix to form a new type of organic film. Herein, the 8 mM Ag₉-NCs/0.3 M L-MA xerogel is introduced into the PMMA, and through the solvent volatilization method to get a hybrid film. Firstly, several films were prepared with different doping concentration of 8 mM Ag₉-NCs/0.3 M L-MA xerogel and it can be observed that as the doping concentration increases (from 0.1% to 0.4%), the fluorescence intensity increases but the transmittance decreases (Figure 4a–c). Integrating transmittance and fluorescence spectra, a composite Ag₉-NCs/L-MA/PMMA film with a mass concentration of 0.3% xerogel was selected to study its sensing performance.

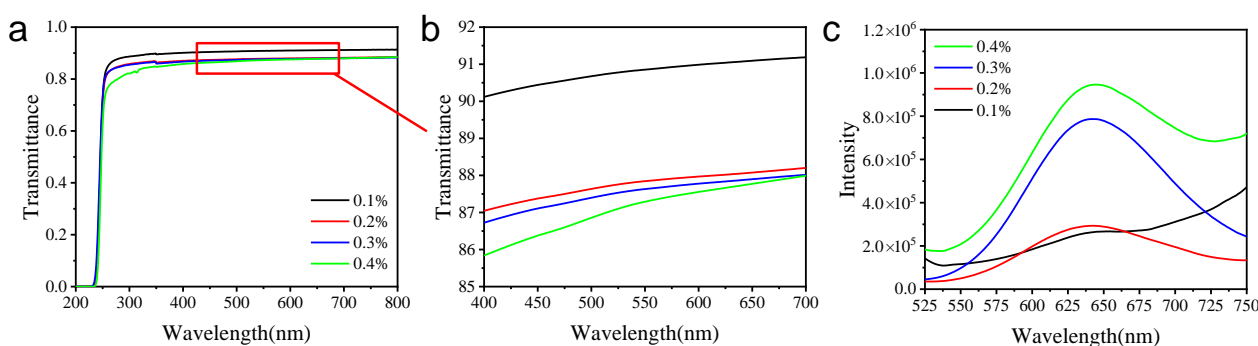


Figure 4. (a) transmittance of films with different doping concentrations. (b) transmittance of films with different doping concentrations (400–700 nm). (c) FL of films with different doping concentrations (from 0.1% to 0.4%).

Then, 0.3% Ag₉-NCs/L-MA xerogel/PMMA films were placed into different metal cation aqueous solutions for 10 min and then, the luminescence spectra of these films were studied (Figures S5 and S6). It is obviously that the composite film shows an obvious quenching effect only toward Fe³⁺ (Figure 5a,b). Furthermore, the 0.3% Ag₉-NCs/L-MA xerogel/PMMA films were placed into aqueous solutions containing different concentrations of Fe³⁺ ions for 10 min to study the corresponding luminescence intensity (Figure 5c,d). With the gradual increase of $c_{\text{Fe}^{3+}}$, the luminescence intensities at 628 nm are significantly weakened. In order to investigate the luminescence quenching efficiency, the Stern–Volmer (S-V) equation was used to quantitatively analyze the quenching curve [32]:

$$I_0/I = 1 + K_{SV}[M] \quad (1)$$

where I_0 and I are the luminescence intensity at 640 nm when $c = 0$ and $c = M$, respectively, K_{SV} is the quenching coefficient of Fe³⁺ ions, and $[M]$ is the molar concentration of Fe³⁺ ions. The quenching curve shows a well-fitted linear relationship at low $c_{\text{Fe}^{3+}}$ (1–100 μM). The K_{SV} value was calculated to be $2.3 \times 10^4 \text{ M}^{-1}$. According to the detection limit expression defined by IUPAC, the detection limit of the composite membrane is calculated to be 0.3 μM , which indicates that the as-prepared 0.3% Ag₉-NCs/L-MA xerogel/PMMA film material exhibited good sensing performance. The limit of detection of the Ag₉-NCs/L-MA xerogel/PMMA film far less than the maximum concentration of Fe(III) in drinking water of 5.36 μM (specified by the Minister of Health of the People’s Republic of China).

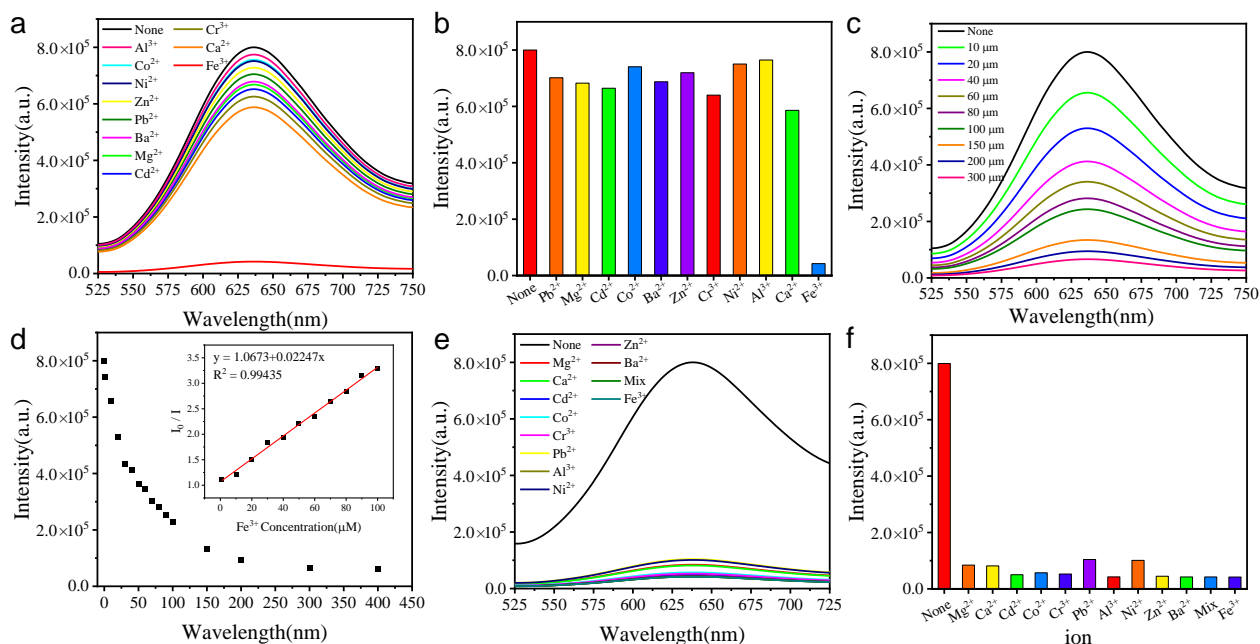


Figure 5. (a) Luminescence emission spectra and (b) luminescence intensities at 640 nm for 0.3% Ag₉-NCs/L-MA xerogel/PMMA film in different cations. (c) Luminescence emission spectra and (d) luminescence intensities at 640 nm for 0.3% Ag₉-NCs/L-MA xerogel/PMMA film in Fe³⁺ with different concentrations. The insert of d shows Stern–Volmer quenching curve of the luminescence intensity of 0.3% Ag₉-NCs/L-MA xerogel/PMMA film at 640 nm against Fe³⁺ concentration; (e) luminescent emission spectra and (f) luminescence intensities at 640 nm for 0.3% Ag₉-NCs/L-MA xerogel/PMMA film in solutions of different cations with Fe³⁺.

High sensitivity and high selectivity are the basic requirements of fluorescence sensors. Various mixed metal cation solutions containing Fe³⁺ (1.0 equivalent) and different competing cations (1.0 equivalent) were prepared for competition experiments. By comparing the fluorescence intensity of 0.3% Ag₉-NCs/L-MA xerogel/PMMA film in different mixed metal cation solutions (Figure 5e,f), it can be seen that the fluorescence is still quenched in the presence of other competing metal cations, which indicates that the composite film has satisfactory selectivity for Fe³⁺ detection. In addition, the used films were picked out and washed with distilled water several times, and the corresponding luminescence intensities cannot be recovered. Therefore, it would be used as a disposable test strip for detection Fe³⁺ ions in drinking water in the future.

The possible sensing mechanism of Fe³⁺ ions quenching the fluorescence of 0.3% Ag₉-NCs/L-MA xerogel/PMMA film was further analyzed. It can be seen from UV-Vis (Figure 6a) that the absorption peaks of Fe³⁺ and the Ag₉-NCs/L-MA hydrogel overlap in the absorption range, indicating that the competitive absorption of Fe³⁺ reduces the energy transfer efficiency [42]. Moreover, structural collapse or change maybe also cause the luminescence to be quenched [32]. The XRD test was performed on the Ag₉-NCs/L-MA xerogel before and after immersion in Fe³⁺ ion aqueous solution (Figure 6b). The XRD spectra of the samples were not consistent, which means that the structure of the Ag₉-NCs/L-MA xerogel was destroyed after treated by Fe³⁺ ion aqueous solution. Therefore, the collapse of the crystal structure is also one of the reasons for the quenching of luminescence. Thus, it can be concluded that the fluorescence quenching of Ag₉-NCs/L-MA xerogel/PMMA film is caused by the competitive absorption of Fe³⁺ and the destruction of the crystal structure. The fluorescence quenching phenomenon of the Ag₉-NCs/L-MA xerogel/PMMA film is shown in Scheme 1.

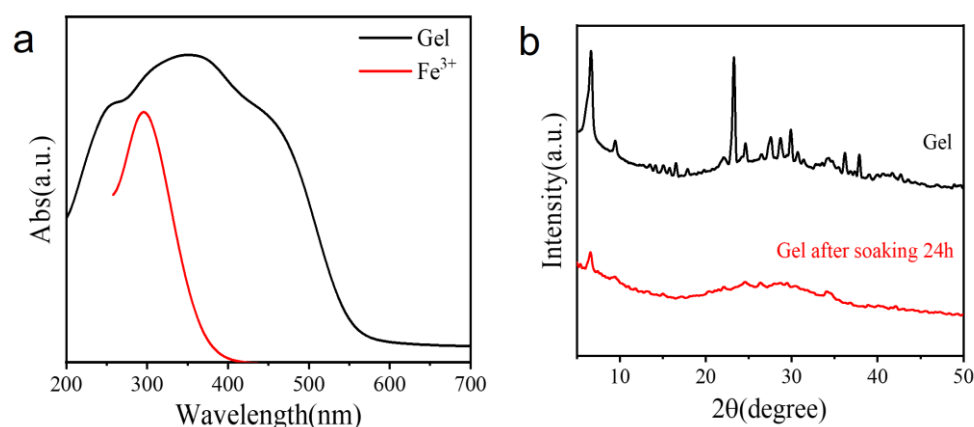


Figure 6. (a) UV-Vis absorption of hydrogel and Fe^{3+} . (b) XRD of xerogel and xerogel after Fe^{3+} soaking 24 h.

3. Conclusions

In summary, through self-assembly, $\text{Ag}_9\text{-NCs}$, and L-MA formed a supramolecular hydrogel, with highly ordered aggregates, by regulating a variety of non-covalent interactions. The nanostructure (tangled hollow tubes) in the hydrogel indicated that L-MA restricts the intramolecular vibration and rotation of the ligand of the $\text{Ag}_9\text{-NCs}$, so that it can emit a stable and bright orange-red phosphorescent emission. The excellent photoluminescence properties of $\text{Ag}_9\text{-NCs/L-MA}$ xerogel make it likely to be used as highly sensitive probes for Fe^{3+} . The $\text{Ag}_9\text{-NCs/L-MA}$ xerogel/PMMA composite film can selectively identify Fe^{3+} , the quenching coefficient K_{SV} is $2.3 \times 10^4 \text{ M}^{-1}$, and the detection limit is $0.3 \mu\text{M}$. The composite film also possesses good recyclability and anti-interference ability, with respect to another ions. The current research aims to achieve AIE, by precisely regulating the formation of ordered aggregates of metal NCs, broadening the research field of metal NCs, and enriching the practical applications of these luminescent materials.

4. Experiment Section

4.1. Materials

$\text{Ag}_9\text{-NCs}$ was synthesized and purified, according to our previous work, which have a crystal structure [44]. L-MA and D-MA were purchased from Sinopharm Chemical Reagent Co (Shanghai, China) and used without further purification. Ultrapure water used in the experiments, with a resistivity of $18.25 \text{ M}\Omega \text{ cm}^{-1}$, was obtained using a UPH-IV ultrapure water purifier (Sichuan, China). Polymethylmethacrylate (PMMA, average Mw: $\sim 350,000$) was purchased from Sigma-Aldrich (Shanghai, China). Dichloromethane (CH_2Cl_2) were obtained from local supplier with the quality of analytical grade and used without further purification.

4.2. Synthesis of $\text{Ag}_9\text{-NCs/L-MA}$ Hybrid Nanostructures

In this experiment, 0.5 mL of $\text{Ag}_9\text{-NCs}$ solution (15.87 mM) was added to 0.5 mL L-MA solution (0.6 M) with stirring. The hydrogel was successfully prepared after 8 h of constant temperature ($20 \text{ }^\circ\text{C}$) in a thermostat. The hydrogels was lyophilized in a vacuum extractor at $60 \text{ }^\circ\text{C}$ for 5 day to collect the orange-yellow powder.

4.3. Fabrication of $\text{Ag}_9\text{-NCs/L-MA/PMMA}$ Composite Thin Film

The PMMA powder (200 mg) was dissolved in dichloromethane (8 mL), then followed by addition of the corresponding required of orange-yellow $\text{Ag}_9\text{-NCs/L-MA}$ xerogels. After being evenly dispersed, place it in a petri dish with a diameter of 6 cm at room temperature for 5 h. Each set of data has been measured 3 times using different batches of film to reduce the error.

4.4. Characterization

A copper mesh was inserted into the gel to obtain a sample and, after drying under an IR lamp for 45 min, TEM images were observed under a JCR-100CX II (JEOL) microscope. The gel was placed on a silica wafer, dried for 45 min under an IR lamp, and observed by field-emission SEM and AFM, respectively. UV–vis data were recorded on a Shimadzu UV-2600 spectrophotometer. Fluorescence data were tested on an LS-55 spectrofluorometer (PerkinElmer, Waltham, MA, USA) and an Edinburgh Instruments FLS920 luminescence spectrometer (xenon lamp, 450 W), respectively. SAXS measurements were performed using an Anton-Paar SAX Sess mc² system with nickel-filtered Cu K α radiation (1.54 Å) operating at 50 kV and 40 mA. XRD patterns were taken on a D8 ADVANCE (Germany Bruker) diffractometer, equipped with Cu K α radiation and a graphite monochromator. FT-IR spectra in KBr wafer were recorded on a VERTEX-70/70v spectrophotometer. CLSM observations were performed using an inverted microscope (model IX81, Olympus, Tokyo, Japan), equipped with a high-numerical-aperture 60 oil-immersed objective lens. The rheological measurements were carried out on an Anton-Paar Physica MCR302 rheometer with a cone–plate system. Before the frequency sweep, an amplitude sweep at a fixed frequency of 1 Hz was carried out to ensure that the selected stress was in the linear viscoelastic region. The frequency sweep was carried out from 0.01 to 100 Hz at a fixed stress of 10 Pa. TGA was performed under a nitrogen atmosphere at 25–700 °C, with a heating speed of 10 °C min^{−1} on a TA SDT Q600 thermal analyzer. CD spectra were obtained using a JASCO J-810 spectropolarimeter, which was flushed with nitrogen during operation. The absolute fluorescence quantum yields were measured with a spectrofluorometer (FLSP920, Edinburgh Instruments Ltd., Livingston, UK), equipped with an integrating sphere.

Supplementary Materials: The following are available online at <https://www.mdpi.com/article/10.3390/gels7040192/s1>, Figure S1: The molecular structure of Ag₉-NCs, Figure S2: AFM image of fibers, Figure S3: (a–b) TEM image of the fibers. (c–d) SEM image of fibers, Figure S4: Elastic modulus (G′) and viscous modulus (G′′) as a function of the applied stress at a constant frequency (1.0 Hz), Figure S5: Photographs of Ag₉-NCs/L–MA xerogel/PMMA film under different conditions, Figure S6: Luminescence emission spectra of 0.3% Ag₉-NCs/L–MA xerogel/PMMA film in 100 μM Fe³⁺ aqueous solution with different interaction time, Table S1: The average lifetime of Ag₉-NCs and hydrogel.

Author Contributions: X.L.: Investigation, methodology, writing—original draft, formal analysis; C.L.: investigation, methodology, formal analysis; Z.W.: investigation, methodology; N.Z.: investigation, methodology, formal analysis; N.F.: investigation, formal analysis; W.W.: investigation, formal analysis; X.X.: conceptualization, resources, writing—review & editing, funding acquisition, supervision. All authors have read and agreed to the published version of the manuscript.

Funding: This research received no external funding.

Acknowledgments: We gratefully acknowledge the financial support from the National Natural Science Foundation of China (21972077), and Key Technology Research and Development Program of Shandong (2019GGX102019).

Conflicts of Interest: The authors declare no conflict of interest.

References

1. Wu, Z.; Jin, R. On the ligand's role in the fluorescence of gold nanoclusters. *Nano Lett.* **2010**, *10*, 2568–2573. [[CrossRef](#)] [[PubMed](#)]
2. Cuaran-Acosta, D.; Londono-Larrea, P.; Zaballos-Garcia, E.; Perez-Prieto, J. Reversible pH-induced fluorescence colour change of gold nanoclusters based on pH-regulated surface interactions. *Chem. Commun.* **2019**, *55*, 1604–1606. [[CrossRef](#)] [[PubMed](#)]
3. Qiao, Y.; Xu, T.; Zhang, Y.; Zhang, C.; Shi, L.; Zhang, G.; Shuang, S.; Dong, C. Green synthesis of fluorescent copper nanoclusters for reversible pH-sensors. *Sens. Actuators B* **2015**, *220*, 1064–1069. [[CrossRef](#)]
4. Wang, W.; Zhan, L.; Du, Y.Q.; Leng, F.; Chang, Y.; Gao, M.X.; Huang, C.Z. Label-free DNA detection on the basis of fluorescence resonance energy transfer from oligonucleotide-templated silver nanoclusters to multi-walled carbon nanotubes. *Anal. Methods* **2013**, *5*, 5555. [[CrossRef](#)]
5. Burratti, L.; De Matteis, F.; Francini, R.; Lim, J.; Scheu, C.; Proposito, P. Fluorescent Silver Nanoclusters Embedded in Hydrogel Matrix and Its Potential Use in Environmental Monitoring. *Appl. Sci.* **2021**, *11*, 3470. [[CrossRef](#)]

6. Yuan, X.; Tay, Y.; Dou, X.; Luo, Z.; Leong, D.T.; Xie, J. Glutathione-protected silver nanoclusters as cysteine-selective fluorometric and colorimetric probe. *Anal. Chem.* **2013**, *85*, 1913–1919. [[CrossRef](#)]
7. Liu, Y.; Ai, K.; Cheng, X.; Huo, L.; Lu, L. Gold-Nanocluster-Based Fluorescent Sensors for Highly Sensitive and Selective Detection of Cyanide in Water. *Adv. Funct. Mater.* **2010**, *20*, 951–956. [[CrossRef](#)]
8. Zhu, X.; Li, Y.; Li, R.; Tu, K.; Li, J.; Xie, Z.; Lei, J.; Liu, D.; Qu, D. Self-assembled N-doped carbon with a tube-in-tube nanostructure for lithium-sulfur batteries. *J. Colloid. Interface Sci.* **2020**, *559*, 244–253. [[CrossRef](#)]
9. Shang, L.; Dong, S.; Nienhaus, G.U. Ultra-small fluorescent metal nanoclusters: Synthesis and biological applications. *Nano Today* **2011**, *6*, 401–418. [[CrossRef](#)]
10. Diez, I.; Pusa, M.; Kulmala, S.; Jiang, H.; Walther, A.; Goldmann, A.S.; Muller, A.H.; Ikkala, O.; Ras, R.H. Color tunability and electrochemiluminescence of silver nanoclusters. *Angew. Chem. Int. Ed.* **2009**, *48*, 2122–2125. [[CrossRef](#)]
11. Diez, I.; Kanyuk, M.I.; Demchenko, A.P.; Walther, A.; Jiang, H.; Ikkala, O.; Ras, R.H. Blue, green and red emissive silver nanoclusters formed in organic solvents. *Nanoscale* **2012**, *4*, 4434–4437. [[CrossRef](#)] [[PubMed](#)]
12. Niesen, B.; Rand, B.P. Thin film metal nanocluster light-emitting devices. *Adv. Mater.* **2014**, *26*, 1446–1449. [[CrossRef](#)]
13. Yuan, Q.; Wang, Y.; Zhao, L.; Liu, R.; Gao, F.; Gao, L.; Gao, X. Peptide protected gold clusters: Chemical synthesis and biomedical applications. *Nanoscale* **2016**, *8*, 12095–12104. [[CrossRef](#)]
14. Chen, L.Y.; Wang, C.W.; Yuan, Z.; Chang, H.T. Fluorescent gold nanoclusters: Recent advances in sensing and imaging. *Anal. Chem.* **2015**, *87*, 216–229. [[CrossRef](#)]
15. Abbas, M.A.; Kamat, P.V.; Bang, J.H. Thiolated Gold Nanoclusters for Light Energy Conversion. *ACS Energy Lett.* **2018**, *3*, 840–854. [[CrossRef](#)]
16. Shiang, Y.-C.; Huang, C.-C.; Chen, W.-Y.; Chen, P.-C.; Chang, H.-T. Fluorescent gold and silver nanoclusters for the analysis of biopolymers and cell imaging. *J. Mater. Chem.* **2012**, *22*, 12972–12982. [[CrossRef](#)]
17. Yang, L.; Shang, L.; Nienhaus, G.U. Mechanistic aspects of fluorescent gold nanocluster internalization by live HeLa cells. *Nanoscale* **2013**, *5*, 1537–1543. [[CrossRef](#)]
18. Kunwar, P.; Hassinen, J.; Bautista, G.; Ras, R.H.A.; Toivonen, J. Direct Laser Writing of Photostable Fluorescent Silver Nanoclusters in Polymer Films. *ACS Nano* **2014**, *8*, 11165–11171. [[CrossRef](#)]
19. Pourreza, N.; Ghomi, M. In Situ synthesized and embedded silver nanoclusters into poly vinyl alcohol-borax hydrogel as a novel dual mode “on and off” fluorescence sensor for Fe (III) and thiosulfate. *Talanta* **2018**, *179*, 92–99. [[CrossRef](#)]
20. Chen, B.; Li, C.; Zhang, J.; Kan, J.; Jiang, T.; Zhou, J.; Ma, H. Sensing and imaging of mitochondrial viscosity in living cells using a red fluorescent probe with a long lifetime. *Chem. Commun.* **2019**, *55*, 7410–7413. [[CrossRef](#)]
21. Hu, R.; Leung, N.L.; Tang, B.Z. AIE macromolecules: Syntheses, structures and functionalities. *Chem. Soc. Rev.* **2014**, *43*, 4494–4562. [[CrossRef](#)] [[PubMed](#)]
22. Jia, X.; Li, J.; Wang, E. Cu nanoclusters with aggregation induced emission enhancement. *Small* **2013**, *9*, 3873–3879. [[CrossRef](#)] [[PubMed](#)]
23. Zhao, T.; Zhang, S.; Bi, Y.; Sun, D.; Kong, F.; Yuan, Z.; Xin, X. Development and characterisation of multi-form composite materials based on silver nanoclusters and cellulose nanocrystals. *Colloid Surf. A* **2020**, *603*, 125257. [[CrossRef](#)]
24. Zhou, Y.; Zeng, H.C. Simultaneous synthesis and assembly of noble metal nanoclusters with variable micellar templates. *J. Am. Chem. Soc.* **2014**, *136*, 13805–13817. [[CrossRef](#)]
25. Luo, Z.; Yuan, X.; Yu, Y.; Zhang, Q.; Leong, D.T.; Lee, J.Y.; Xie, J. From aggregation-induced emission of Au(I)-thiolate complexes to ultrabright Au(0)@Au(I)-thiolate core-shell nanoclusters. *J. Am. Chem. Soc.* **2012**, *134*, 16662–16670. [[CrossRef](#)]
26. Tan, C.; Qi, X.; Liu, Z.; Zhao, F.; Li, H.; Huang, X.; Shi, L.; Zheng, B.; Zhang, X.; Xie, L.; et al. Self-assembled chiral nanofibers from ultrathin low-dimensional nanomaterials. *J. Am. Chem. Soc.* **2015**, *137*, 1565–1571. [[CrossRef](#)]
27. Hong, X.; Tan, C.; Liu, J.; Yang, J.; Wu, X.J.; Fan, Z.; Luo, Z.; Chen, J.; Zhang, X.; Chen, B.; et al. AuAg nanosheets assembled from ultrathin AuAg nanowires. *J. Am. Chem. Soc.* **2015**, *137*, 1444–1447. [[CrossRef](#)]
28. Xia, Y.; Nguyen, T.D.; Yang, M.; Lee, B.; Santos, A.; Podsiadlo, P.; Tang, Z.; Glotzer, S.C.; Kotov, N.A. Self-assembly of self-limiting monodisperse supraparticles from polydisperse nanoparticles. *Nat. Nanotechnol.* **2011**, *6*, 580–587. [[CrossRef](#)]
29. Wu, Z.; Yao, Q.; Zang, S.; Xie, J. Directed Self-Assembly of Ultrasmall Metal Nanoclusters. *ACS Mater. Lett.* **2019**, *1*, 237–248. [[CrossRef](#)]
30. Shen, J.; Wang, Z.; Sun, D.; Xia, C.; Yuan, S.; Sun, P.; Xin, X. pH-Responsive Nanovesicles with Enhanced Emission Co-Assembled by Ag(I) Nanoclusters and Polyethyleneimine as a Superior Sensor for Al(3). *ACS Appl. Mater. Interfaces* **2018**, *10*, 3955–3963. [[CrossRef](#)]
31. Wu, Z.; Liu, J.; Gao, Y.; Liu, H.; Li, T.; Zou, H.; Wang, Z.; Zhang, K.; Wang, Y.; Zhang, H.; et al. Assembly-Induced Enhancement of Cu Nanoclusters Luminescence with Mechanochromic Property. *J. Am. Chem. Soc.* **2015**, *137*, 12906–12913. [[CrossRef](#)]
32. Chen, W.; Fan, R.; Fan, J.; Liu, H.; Sun, T.; Wang, P.; Yang, Y. Lanthanide Coordination Polymer-Based Composite Films for Selective and Highly Sensitive Detection of Cr₂O₇²⁻ in Aqueous Media. *Inorg. Chem.* **2019**, *58*, 15118–15125. [[CrossRef](#)]
33. Liu, L.; Li, Z.; Liu, Y.; Zhang, S.X.-A. Recent advances in film-based fluorescence sensing. *Sci. Sin. Chim.* **2019**, *50*, 39–69. [[CrossRef](#)]
34. Bhasin, A.K.K.; Chauhan, P.; Chaudhary, S. A novel sulfur-incorporated naphthoquinone as a selective “turn-on” fluorescence chemical sensor for rapid detection of Ba²⁺ ion in semi-aqueous medium. *Sens. Actuators B* **2019**, *294*, 116–122. [[CrossRef](#)]
35. Song, C.; Liu, Y.; Jiang, X.; Zhang, J.; Dong, C.; Li, J.; Wang, L. Ultrasensitive SERS determination of avian influenza A H7N9 virus via exonuclease III-assisted cycling amplification. *Talanta* **2019**, *205*, 120137. [[CrossRef](#)]
36. Aysha, T.S.; El-Sedik, M.S.; Mohamed, M.B.I.; Gaballah, S.T.; Kamel, M.M. Dual functional colorimetric and turn-off fluorescence probe based on pyrrolinone ester hydrazone dye derivative for Cu²⁺ monitoring and pH change. *Dyes Pigment.* **2019**, *170*, 107549. [[CrossRef](#)]

37. Li, J.J.; Qiao, D.; Zhao, J.; Weng, G.J.; Zhu, J.; Zhao, J.W. Ratiometric fluorescence detection of Hg²⁺ and Fe³⁺ based on BSA-protected Au/Ag nanoclusters and His-stabilized Au nanoclusters. *Methods Appl. Fluoresc.* **2019**, *7*, 045001. [[CrossRef](#)]
38. Li, Y.; Li, Y.; Duan, J.; Hou, J.; Hou, Q.; Yang, Y.; Li, H.; Ai, S. Rapid and ultrasensitive detection of mercury ion (II) by colorimetric and SERS method based on silver nanocrystals. *Microchem. J.* **2021**, *161*, 105790. [[CrossRef](#)]
39. Katowah, D.F.; Alqarni, S.; Mohammed, G.I.; Al Sheheri, S.Z.; Alam, M.M.; Ismail, S.H.; Asiri, A.M.; Hussein, M.A.; Rahman, M.M. Selective Hg²⁺ sensor performance based various carbon-nanofillers into CuO-PMMA nanocomposites. *Polym. Adv. Technol.* **2020**, *31*, 1946–1962. [[CrossRef](#)]
40. Sun, P.; Wang, Z.; Bi, Y.; Sun, D.; Zhao, T.; Zhao, F.; Wang, W.; Xin, X. Self-Assembly-Driven Aggregation-Induced Emission of Silver Nanoclusters for Light Conversion and Temperature Sensing. *ACS Appl. Nano Mater.* **2020**, *3*, 2038–2046. [[CrossRef](#)]
41. Sun, P.; Wang, Z.; Sun, D.; Bai, H.; Zhu, Z.; Bi, Y.; Zhao, T.; Xin, X. pH-guided self-assembly of silver nanoclusters with aggregation-induced emission for rewritable fluorescent platform and white light emitting diode application. *J. Colloid Interface Sci.* **2020**, *567*, 235–242. [[CrossRef](#)]
42. Cheng, X.; Sun, P.; Zhang, N.; Zhou, S.; Xin, X. Self-assembly of silver nanoclusters and phthalic acid into hollow tubes as a superior sensor for Fe³⁺. *J. Mol. Liq.* **2021**, *323*, 115032. [[CrossRef](#)]
43. Barreiro, E.; Casas, J.S.; Couce, M.D.; Laguna, A.; López-de-Luzuriaga, J.M.; Monge, M.; Sánchez, A.; Sordo, J.; Vázquez López, E.M. A novel hexanuclear silver(i) cluster containing a regular Ag₆ ring with short Ag–Ag distances and an argentophilic interaction. *Dalton Trans.* **2013**, *42*, 5916. [[CrossRef](#)]
44. Xie, Z.; Sun, P.; Wang, Z.; Li, H.; Yu, L.; Sun, D.; Chen, M.; Bi, Y.; Xin, X.; Hao, J. Metal-Organic Gels from Silver Nanoclusters with Aggregation-Induced Emission and Fluorescence-to-Phosphorescence Switching. *Angew. Chem. Int. Ed.* **2020**, *59*, 9922–9927. [[CrossRef](#)]